

Electronic Supporting Information

A simple, efficient and selective catalyst for closed-loop recycling of PEF in situ towards a circular material economy approach

Shaowei Wu,^{a,b,c} Lu Li,^{*a,c} Lei Song,^{a,c} Guannan Zhou,^{a,c} Lixin Liu,^{a,c} Hailan Kang,^{*b}
Guangyuan Zhou^{a,c} and Rui Wang^{a,c}

^a Division of Energy Materials (DNL 22), Dalian Institute of Chemical Physics, Chinese Academy of Sciences, Dalian, 116023, China

^b Key Laboratory for Rubber Elastomer of Liaoning Province, Shenyang University of Chemical Technology, Shenyang, China

^c Liaoning Key Laboratory of Speciality Polymers, Dalian, China

Experimental section

Chemicals

Analytical grade commercial 2,5-Furandicarboxylic acid (FDCA, >99%), Gallium chloride (GaCl₃, 99.99%), Gallium oxide (β -Ga₂O₃, 99.99%), titanium(IV) butoxide (TBT, \geq 99%), Trifluoroacetic acid-d (TFA-D, 99.5 atom% D) and Sodium trifluoroacetate (CF₃COONa, 98%) were purchased from Innochem and Shanghai Aladdin Biochemical Technology Co. Ltd, respectively. Ethylene glycol (EG, \geq 99%), Acetone (\geq 99.5%) and Alcohol (\geq 95%) were purchased from Sinopharm Chemical Reagent Co., Ltd. Hexafluoroisopropanol (HFIP, \geq 99.5%) were purchased from Jinan Langhua Chemical Co., Ltd. Polyethylene terephthalate (PET) was purchased from Jinyuan Chemical Co., LTD. All chemicals were analytical grade and used as received without any further purification. Deionized water was used throughout.

Catalyst preparation

1 g of GaCl₃ was added to 150 mL of ethylene glycol and refluxed in an atmosphere of N₂. The reaction was mechanically stirred and heated to reflux prior to adding 0.6 g of water to the reaction flask. The reaction was allowed to proceed for 3 h~12 h prior to cooling to room temperature in a water bath. Acetone was added to the transparent solution to induce aggregation. The precipitate was washed to neutral with alcohol and deionized water, then vacuum dried overnight at the 60 °C. After heating in air at 450 °C for 4 h, the calcined powder was γ -Ga₂O₃-n (n represents the reflux reaction time, h).

Procedure for in-situ closed-loop recovery of PEF

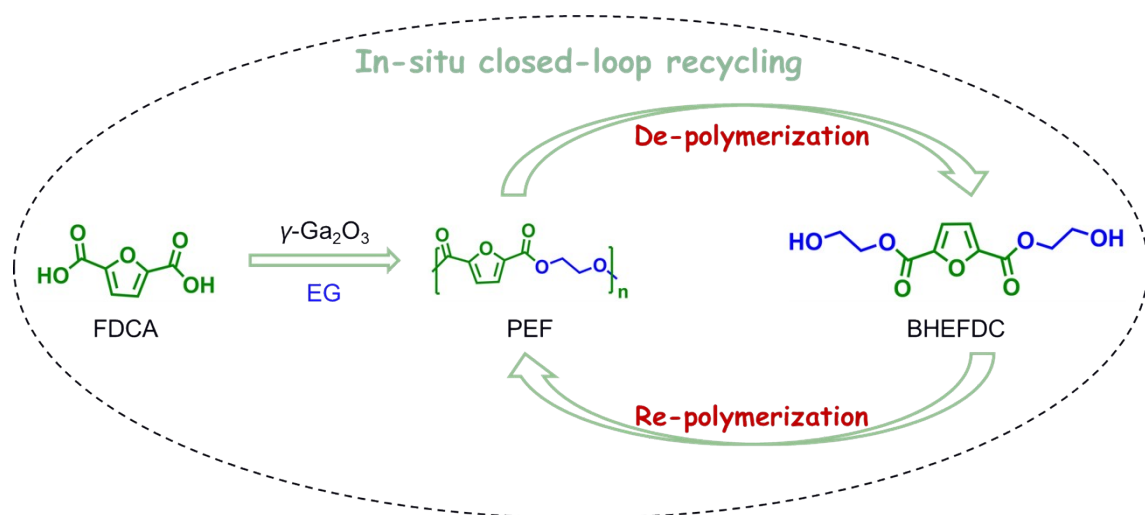
The in-situ closed-loop recycling procedure (Scheme S1) started with the polyesterification reaction, a

direct esterification method involving a two-step (esterification and polycondensation) process, where FDCA, EG (molar ratio FDCA/EG=1:1.7) and γ -Ga₂O₃ nanoparticles (0.1 mol% based on FDCA) were put in a three-necked glass flask, with mechanical stirring at the speed of 200 rpm. The esterification was carried out at 190 °C for 1 h, 200 °C for 1 h and 210 °C for 1 h, respectively, until no more by-product H₂O was distilled. The polycondensation was conducted at 240 °C for 3 h under high vacuum with the pressure reduced to less than 100 Pa to remove the excess EG. After the polycondensation reaction was completed, the PEF were prepared. TBT and β -Ga₂O₃ catalyst was used for comparison experiments.

This is followed by in-situ de-polymerization, glycolysis, in a three-necked glass flask fitted with a spherical condenser, under magnetic agitation and nitrogen atmosphere. Typically, W g of PEF powder (γ -Ga₂O₃ catalyzed synthesis) and EG were mixed in glass flask. The reactions were carried out at 180 °C for 2h, with mass ratio of PEF/EG PEF/EG= 1/4. At the end of the reaction, the glass flask was cooled in ice water. Subsequently, dimethyl sulfoxide was added to dissolve the resulting product, which was allowed to stand for a period. The supernatant was analyzed using high-performance liquid chromatography (HPLC) to determine the product yield. The precipitate was then washed with ethanol, dried, and weighed to calculate the degradation rate of PEF. The degradation rate of PEF (Equation S1) was calculated using the following formula:

$$PEF \text{ weight loss } (\%) = \frac{\text{initial weight of PEF } (g) - \text{weight of residual PEF } (g)}{\text{initial weight of PEF } (g)} \times 100\% \quad (S1)$$

Continuously, the unpurified reaction products, still containing γ -Ga₂O₃, were directly utilized in the polyesterification reaction. A high vacuum was maintained for 3 h while the temperature was gradually increased to 240 °C. Upon completion of the reaction, the starting polymer (rPEF) was obtained. This process successfully completes a comprehensive in-situ closed-loop recycling system.



Scheme S1. In situ closed-loop chemical recovery of PEF via oxygen vacancy defect state γ -Ga₂O₃ nanoparticles.

PEF glycolysis products post-processing procedures

Upon completion of the glycolysis reaction, the reactor was cooled quickly in an ice water bath to quench the reaction. After the obtained mixture is refrigerated at minus 10 °C for a period of time, the furan-based oligomers precipitated and could be separated from the EG phase. The separated precipitate can be washed with deionized water and filtered to obtain solid I. Then, the remaining filtrate after filtration is concentrated using a rotary evaporator, and the concentrated solution is also refrigerated for a period of time. After new solid precipitates, solid II can be obtained through the same treatment method. Finally, the two solid products I and II obtained from in-situ glycolysis of PEF were tested and analyzed for their composition after vacuum drying at 60 °C.

Characterization

The morphology of the synthesized product was observed using the transmission electron microscope (TEM) images were recorded using a JEOL JEM 2000 Fx-11 at an acceleration voltage of 200 kV equipped. Structural analysis was performed using Bruker Germany D8 Advanced X-ray powder diffractometer (XRD) with Cu K α radiation ($k = 1.5406 \text{ \AA}$). The scan range was from 5 to 80° (2θ) with a step of 0.02° and a scan rate of 7.5° min⁻¹. X-ray photoelectron spectroscopy (XPS) measurements were performed using ESCA + Omicron UK XPS system with Mg K α source and photon energy 1486.6 eV. Low-temperature electron paramagnetic resonance (EPR) spectra were acquired on a Bruker EMX EPR spectrometer (Billerica, MA) at 77K in a vacuum. Thermogravimetric analysis was carried out using TA instruments (Q600 SDT) from room temperature to 800 °C at a heating rate of 10 °C/min. Nitrogen adsorption–desorption isotherms were obtained using a Belsorp HP surface area analyzer at 77 K. Prior to the measurement, the samples were degassed at 393 K for 12 h. The Brunner–Emmett–Teller surface area (SBET) was calculated from the adsorption branch in the p/p_0 range of 0.005–0.1, and the pore size distribution was calculated using nonlocal density functional theory (NLDFT), which was based on N₂ adsorption at 77 K on carbon (slit/cylinder pore, NLDFT equilibrium model). Temperature-Programmed Desorption of NH₃ (NH₃-TPD) experiments were carried out using AutoChem II-OmniStar. First, ca. 100 mg of samples were pre-treated for 1 h in N₂ flow at 300 °C to remove strongly bound species (H₂O and CO₂), then cooled to 100 °C and saturated with continuously flowing ammonia (10 % NH₃/N₂). Afterward, the sample was purged by N₂ at 100 °C for 0.5 h to eliminate the physical adsorbed ammonia, then cooled to 50 °C. Finally, the sample was heated to 700 °C at a rate of 10 °C/min in N₂. The final temperature was maintained for 30 min to achieve complete desorption. All total gas flow is 50 mL/min.

Nuclear Magnetic Resonance Spectroscopy (^1H NMR) measurement was carried out on a Bruker Avance 400-MHz NMR spectrometer. PEF was dissolved in trifluoroacetic acid-d (TFA). Weight-average molecular weight (M_w), number-average molecular weight (M_n), and the distribution (\mathcal{D}) of PEF were obtained by gel permeation chromatography using a liner hexafluoroisopropanol (HFIP) column and a Waters 515 HPLC with OPTILAB DSP interferometric refractometer (Wyatt Technology) as detector. The eluent was HFIP at a flow rate of 1.0 mL/min at 35 °C. Mono dispersed polymethyl methacrylate was used as the standard samples. Glass-transition temperature and melting behavior were recorded with differential scanning calorimetry (DSC) on a TA-Q 200 thermal analyzer, calibrated with indium standard. PEF samples (6.0 ± 0.5 mg) were heated to 280 °C at a heating rate of 10 °C/min and kept for 3 min in order to erase the thermal history. The melt was cooled to -25 °C and then heated to 280 °C at 10 °C/min. The thermal stability was determined by thermogravimetric analysis (TGA) using TA-TGA 55 series apparatus. Samples (6.0 ± 0.5 mg) were heated by a single-step thermal process (30 °C-700 °C, 10 °C/min).

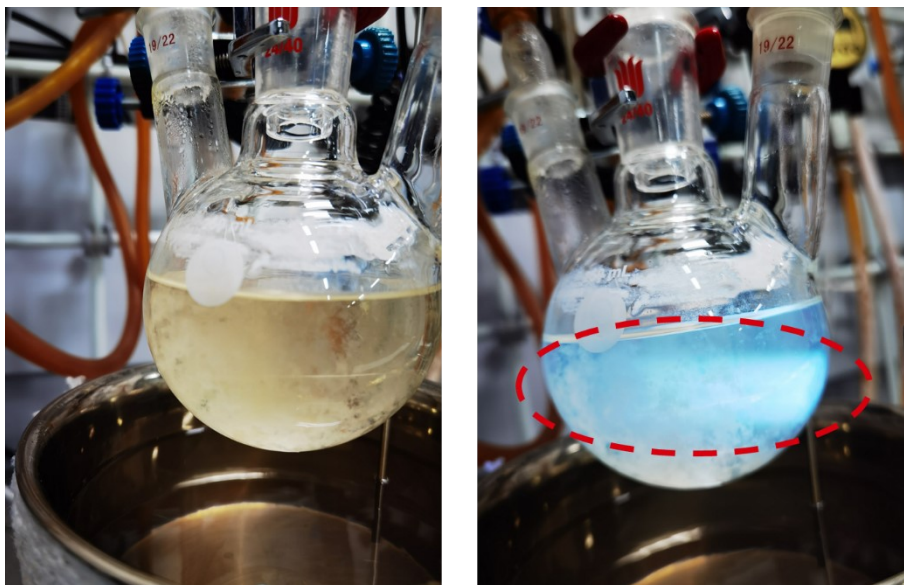


Fig. S1 A significant Tindall effect was observed under UV irradiation.

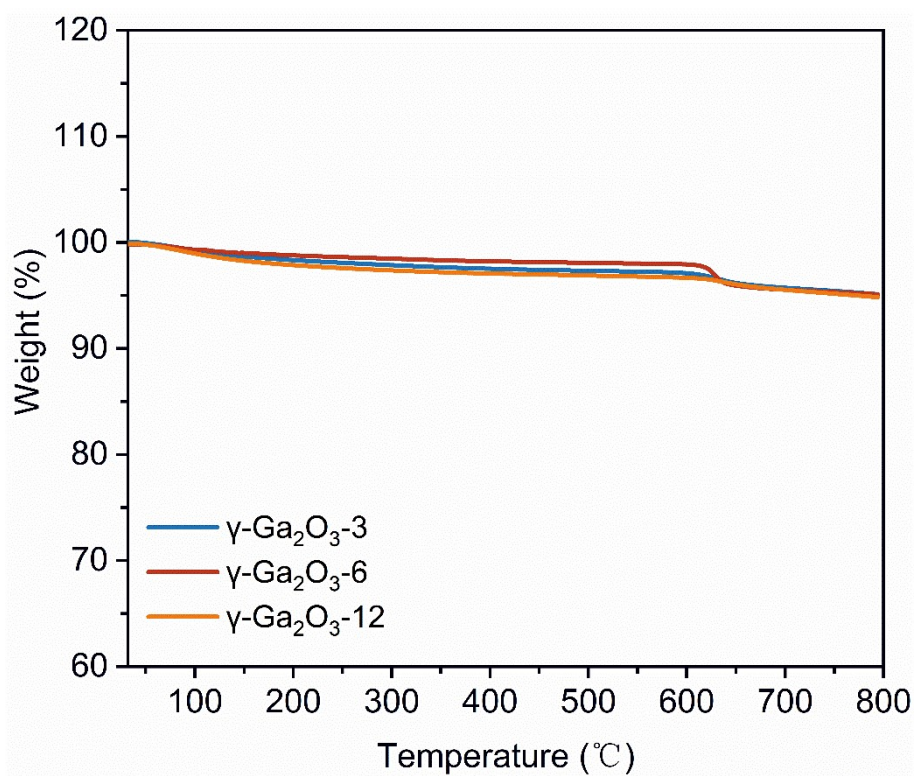


Fig. S2 TGA curves of oxygen-vacancy defective γ -Ga₂O₃-n catalysts (n represents the reflux reaction time in hours).

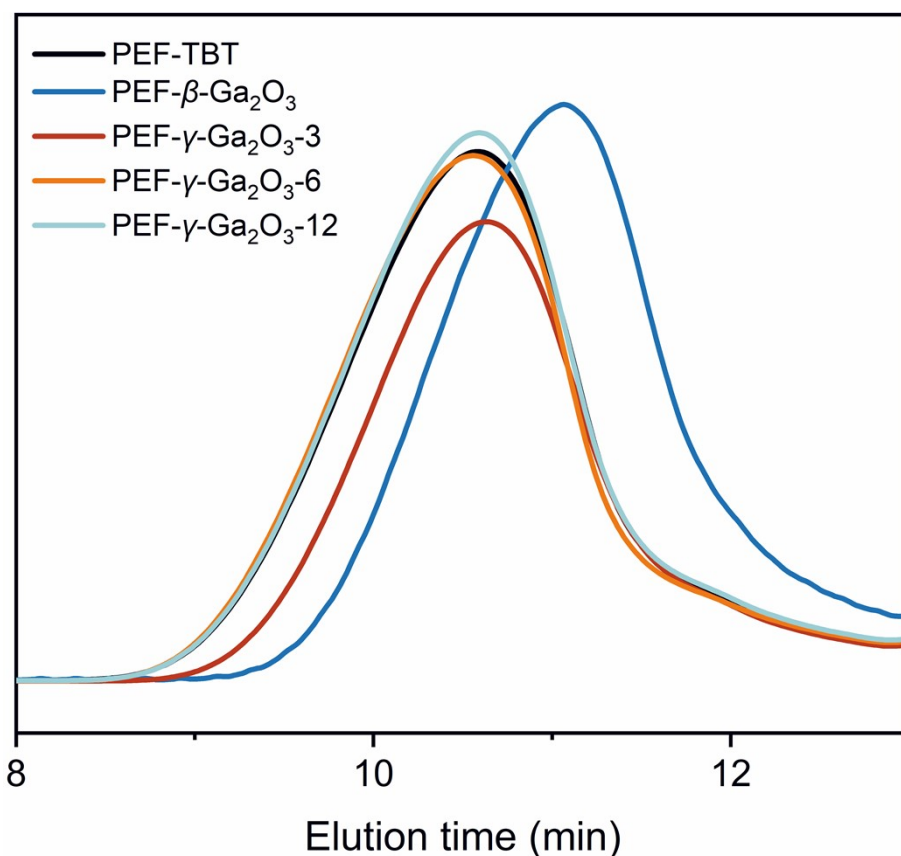


Fig. S3 GPC curves of PEF synthesized by different catalysts.

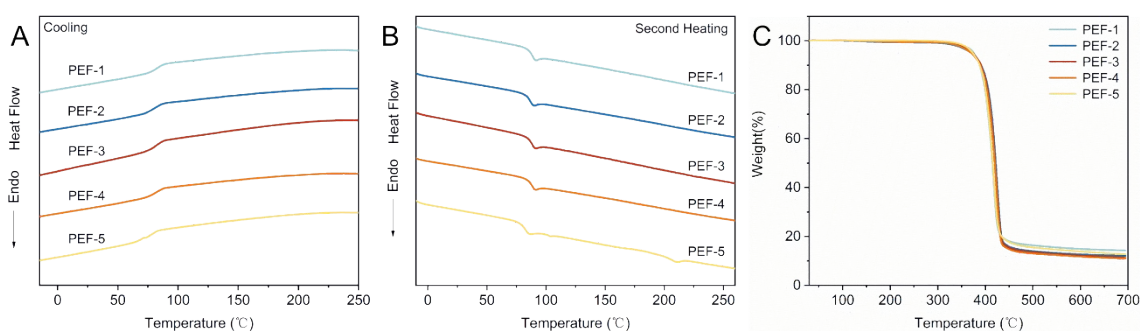


Fig. S4 (A), (B) DSC curves and (C) TGA curves of PEFs catalyzed by TBT catalysts (PEF-1), oxygen vacancy defective γ - Ga_2O_3 - n catalysts (PEF-2~4) and β - Ga_2O_3 catalysts (PEF-5).

The kinetics of FDCA and EG catalyzed by γ - Ga_2O_3 nanoparticles

The relationship between $[\eta]$ of PEFs and time in polycondensation stage was studied. The esterification was carried out at 190 °C for 1 h, 200 °C for 1 h and 210 °C for 1 h, respectively, until no more by-product H_2O was distilled. Subsequently, the polycondensation was conducted at 240 °C with the pressure slowly reduced to less than 100 kPa in half an hour for 1 h, 2 h, 3 h, 4 h and 5 h, respectively. The intrinsic viscosity ($[\eta]$) of PEFs was measured at 25 °C with an Ubbelohde viscometer. The concentration of the polyesters in a mixed solvent, phenol/1,1,2,2-tetrachloroethane (1/1, w/w), was 0.5 g/dL.”

The molecular weight of PEF was expressed by $[\eta]$. As shown in Fig. S5, the $[\eta]$ increased gradually from

0.13 dL/g to 0.81 dL/g with the increase of polycondensation time from 1 h to 3 h. Further prolonging the reaction time to 5 h, the molecular weight ($[\eta]$, increased from 0.81 dL/g to 0.91 dL/g) increased slightly. Taking energy saving and the product color into the consideration, the optimum polycondensation condition was 3 h at 240 °C under high vacuum.

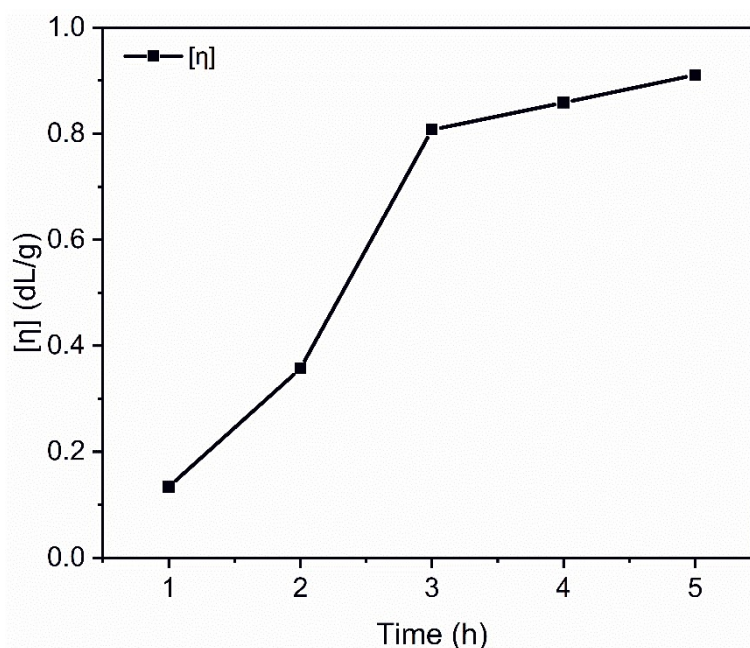


Fig. S5 Effect of polycondensation time on $[\eta]$ of PEFs.

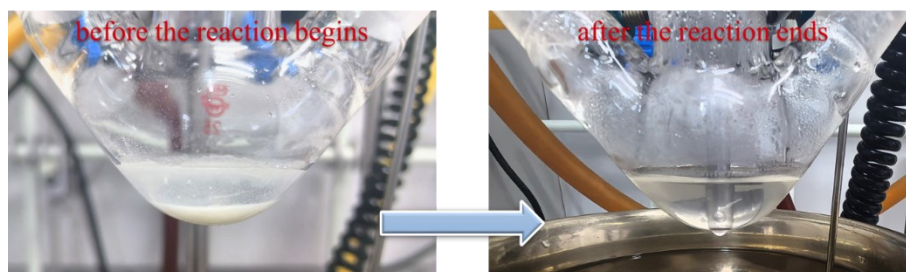


Fig. S6 Comparison diagram of PEF glycolysis reaction before and after

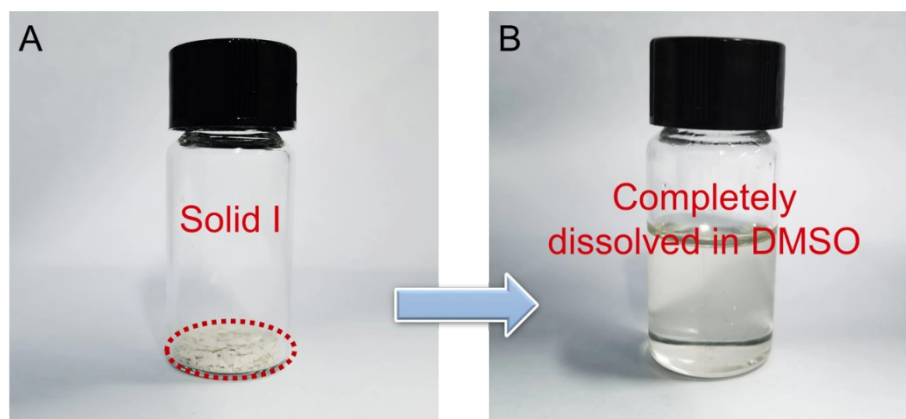


Fig. S7 Dissolution diagram of solid I in DMSO (A) before dissolution; (B) after dissolution.

HPLC-MS analysis of the glycolysis reaction media

High-performance liquid chromatography-mass spectrometry (HPLC-MS) was employed to further analyze the composition of solid II. The mass spectrum depicted in Fig. S8 revealed a peak of highest intensity at $m/z = 63.04$, which is consistent with the molecular weight of protonated glycol (H^+) (Fig. S8A). Similarly, the peak at $m/z = 107.07$ corresponds to the H^+ molecular weight of protonated diethylene glycol (Fig. S8B). Notably, the peak at $m/z = 262.09$ (Fig. S8C) matches the molecular weight of ammonium (NH_4^+) protonated bis(hydroxyethyl)-2,5-furandicarboxylate (BHEFDC), while the peak at $m/z = 444.11$ (Fig. S8D) aligns with the molecular weight of NH_4^+ protonated BHEFDC dimer. These results indicate that solid II is a mixture of BHEFDC and BHEFDC dimer. HPLC analysis reveals that the BHEFDC content reaches 91.3%, establishing it as the predominant component (Fig. S9 and Table S4).

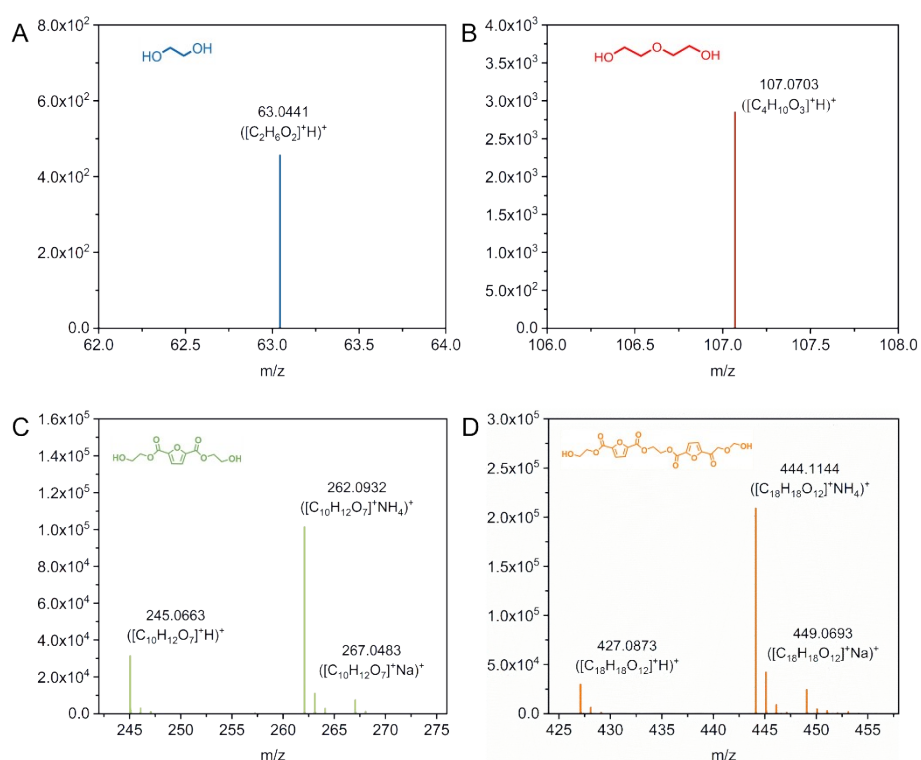


Fig. S8 (A), (B), (C) and (D) MS spectra of Solid II of PEF glycolytic products solid II.

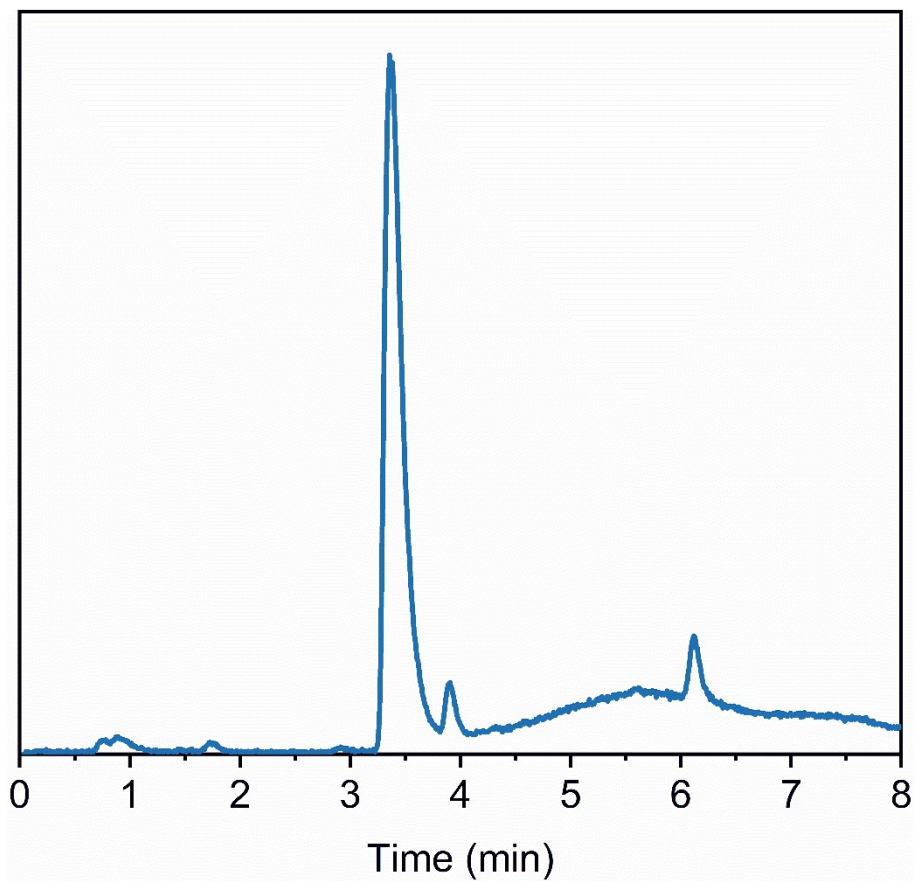


Fig. S9 HPLC chromatogram of PEF glycolysis products solid II: 0.9 min, ethylene glycol and diethylene glycol; 3.4 min, bis(hydroxyethyl)-2,5-furandicarboxylate (BHEFDC) and 6.1 min, BHEFDC dimer.

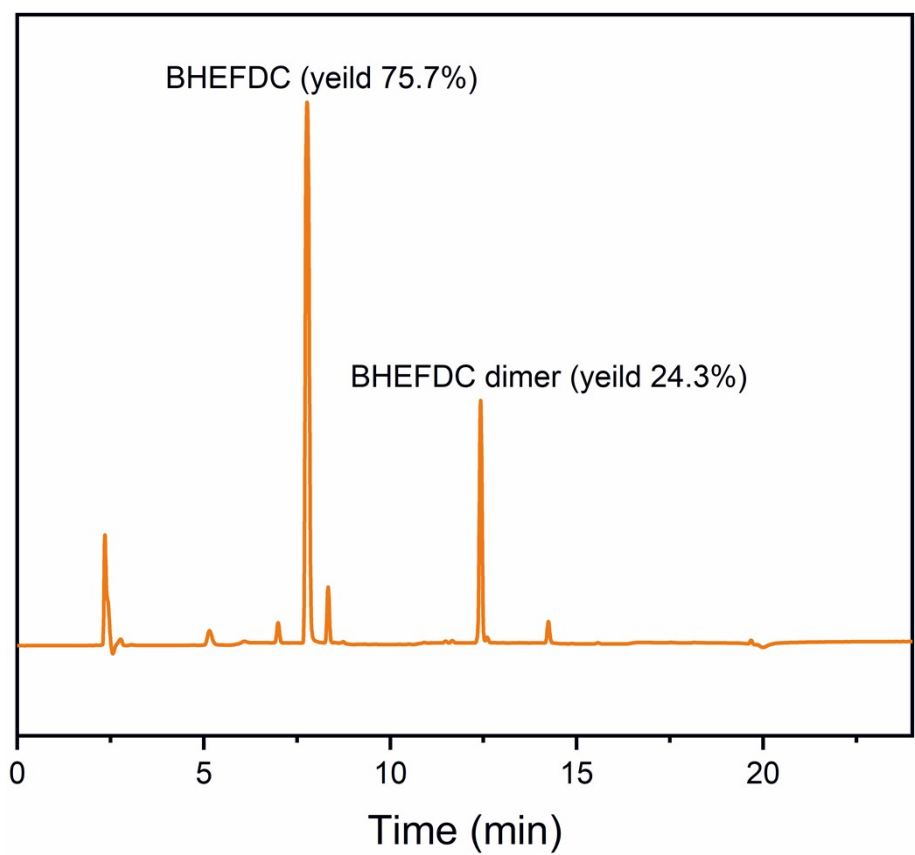


Fig. S10 HPLC chromatogram of PEF glycolysis products (after dissolution by dimethyl sulfoxide): 2.4 min, dimethyl sulfoxide; 7.8 min, bis(hydroxyethyl)-2,5-furandicarboxylate (BHEFDC) and 12.4 min, BHEFDC dimer.

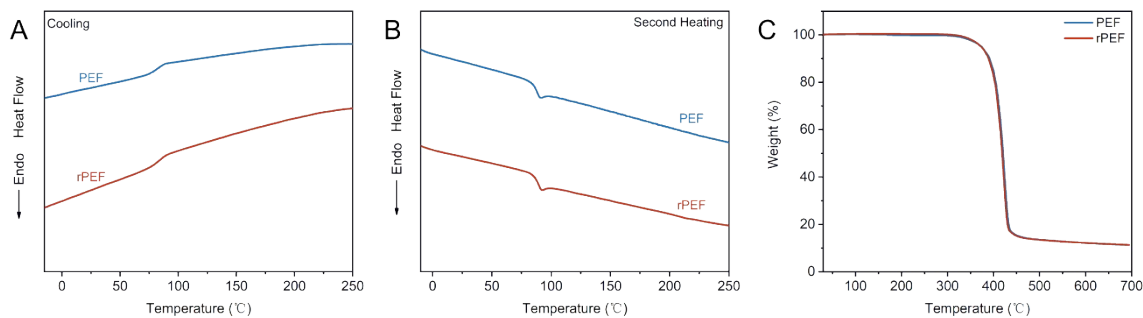


Fig. S11 (A), (B) DSC curves and (C) TGA curves of the re-polymerized PEF (rPEF) and PEF.

Density Functional Theory

Computational methods:

Spin-polarized DFT calculations were performed using the Vienna ab initio simulation package (VASP). The generalized gradient approximation proposed by Perdew, Burke, and Ernzerhof (GGA-PBE) is selected for the exchange-correlation potential. The pseudo-potential was described by the projector-augmented-wave (PAW) method. The geometry optimization is performed until the Hellmann–Feynman force on each atom is smaller than $0.02 \text{ eV} \cdot \text{\AA}^{-1}$. The energy criterion is set to 10^{-6} eV in iterative solution of the Kohn-Sham equation. Dimer method is used to find the transition states.

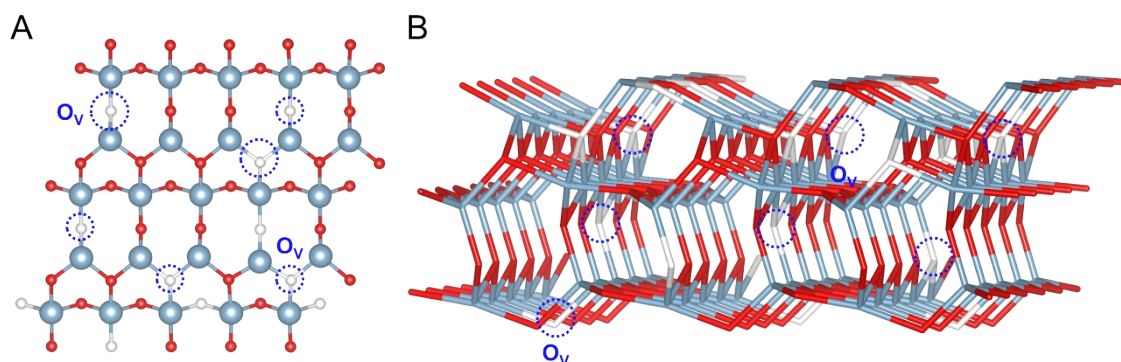


Fig. S12 Top (A) and side (B) views of oxygen-vacancy defective nano-Ga₂O₃ surface structures (the blue, red, and white balls represent the Ga, O atoms, and oxygen vacancy).

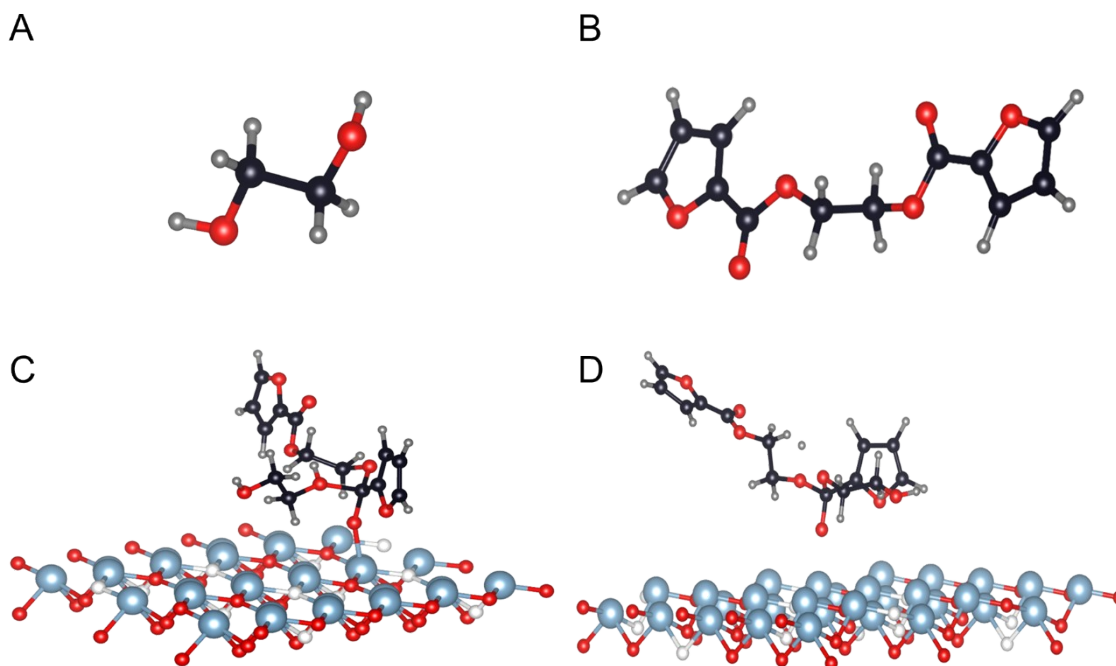


Fig. S13 Small molecular structure formula of (A) Ethylene glycol and (B) Ethane-1,2-diyl bis(furan-2-carboxylate); the determined transition state structures for DFT computational optimization (C) TS 1 and (D) TS 2 (the blue, red, black, gray and white balls represent the Ga, O, C, H atoms, and oxygen vacancy).

To investigate the glycolysis pathway of PET in the presence of γ -Ga₂O₃ catalysts with oxygen vacancy defects, we employed DFT calculations to construct a model of the nano-Ga₂O₃ surface with oxygen vacancies (Fig. S12). To simplify the computational process, ethane-1,2-diyl dibenzoate (TDDZ) was used as a model molecule (Fig. S15). By comparing the energy profiles (Fig. S14B) of the glycolysis reactions of TDDZ and ethane-1,2-diyl bis(furan-2-carboxylate) (EDBFC), it is evident that the energy required for TDDZ to undergo glycolysis on the oxygen-vacancy-rich nano-Ga₂O₃ surface is significantly higher than that for EDBFC, particularly in the rate-determining step (TS1 formation), where the energy barrier for TDDZ is 37.25 kJ mol⁻¹ higher. These DFT results further confirm that the energy required for PET glycolysis is higher than that for PEF under the same catalytic conditions, which explains why PET may not undergo glycolysis as efficiently as PEF under conditions favorable for PEF. Thus, the low selectivity of the γ -Ga₂O₃ catalyst for PET glycolysis observed in our work is justified.

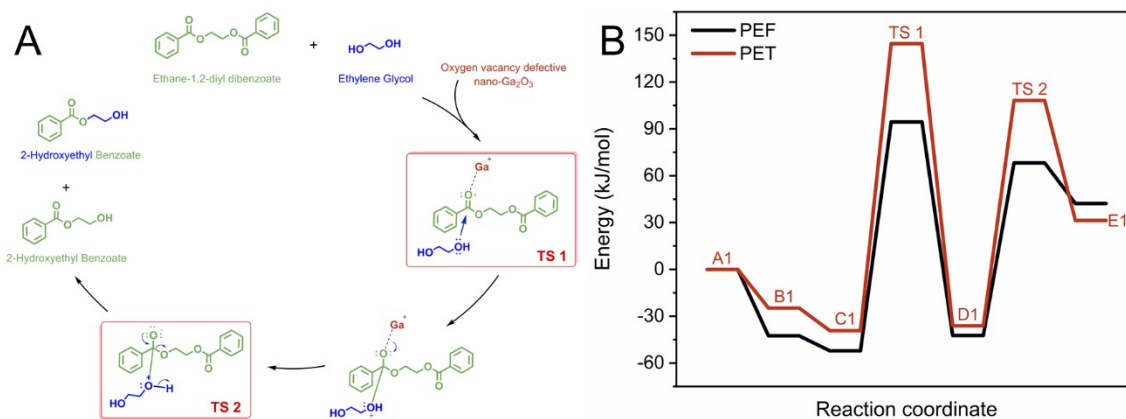


Fig. S14 (A) Modelled activation mechanism for the glycolysis of PET, using ethane-1,2-diyl dibenzoate to mimic PET, ethylene glycol as a nucleophile, and oxygen-vacancy defective nano-Ga₂O₃ as catalyst, yielding 2 2-hydroxyethyl benzoate as products; (B) Energy curve and reaction structure formula of ethane-1,2-diyl bis(furan-2-carboxylate) glycolysis reaction pathway on oxygen-vacancy defective nano-Ga₂O₃ surface.

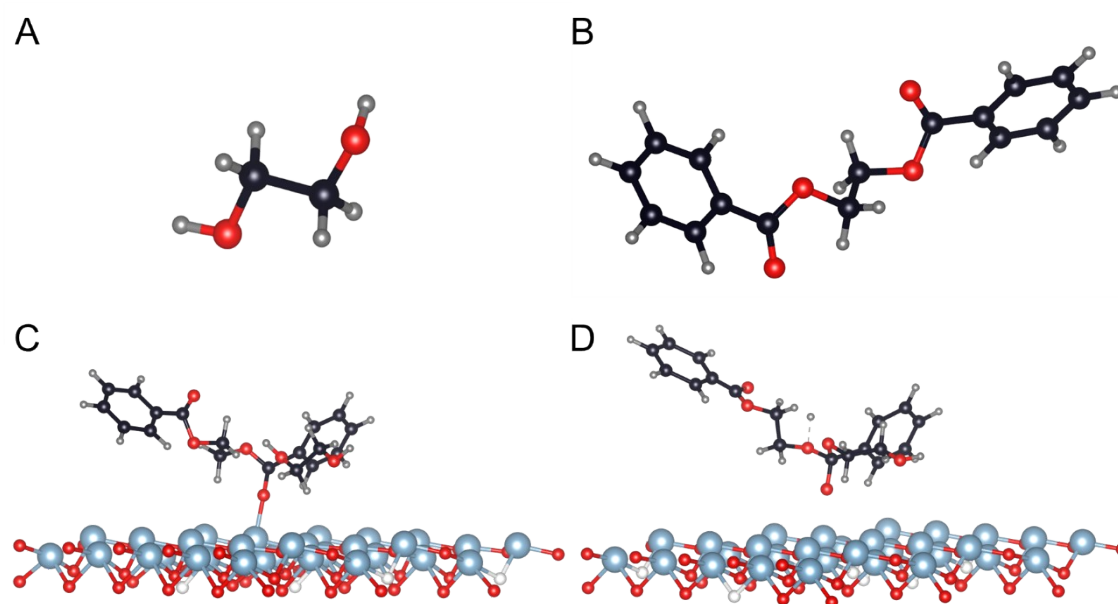


Fig. S15 Small molecular structure formula of (A) Ethylene glycol and (B) Ethane-1,2-diyl dibenzoate; the determined transition state structures for DFT computational optimization (C) TS 1 and (D) TS 2 (the blue, red, black, gray and white balls represent the Ga, O, C, H atoms, and oxygen vacancy).

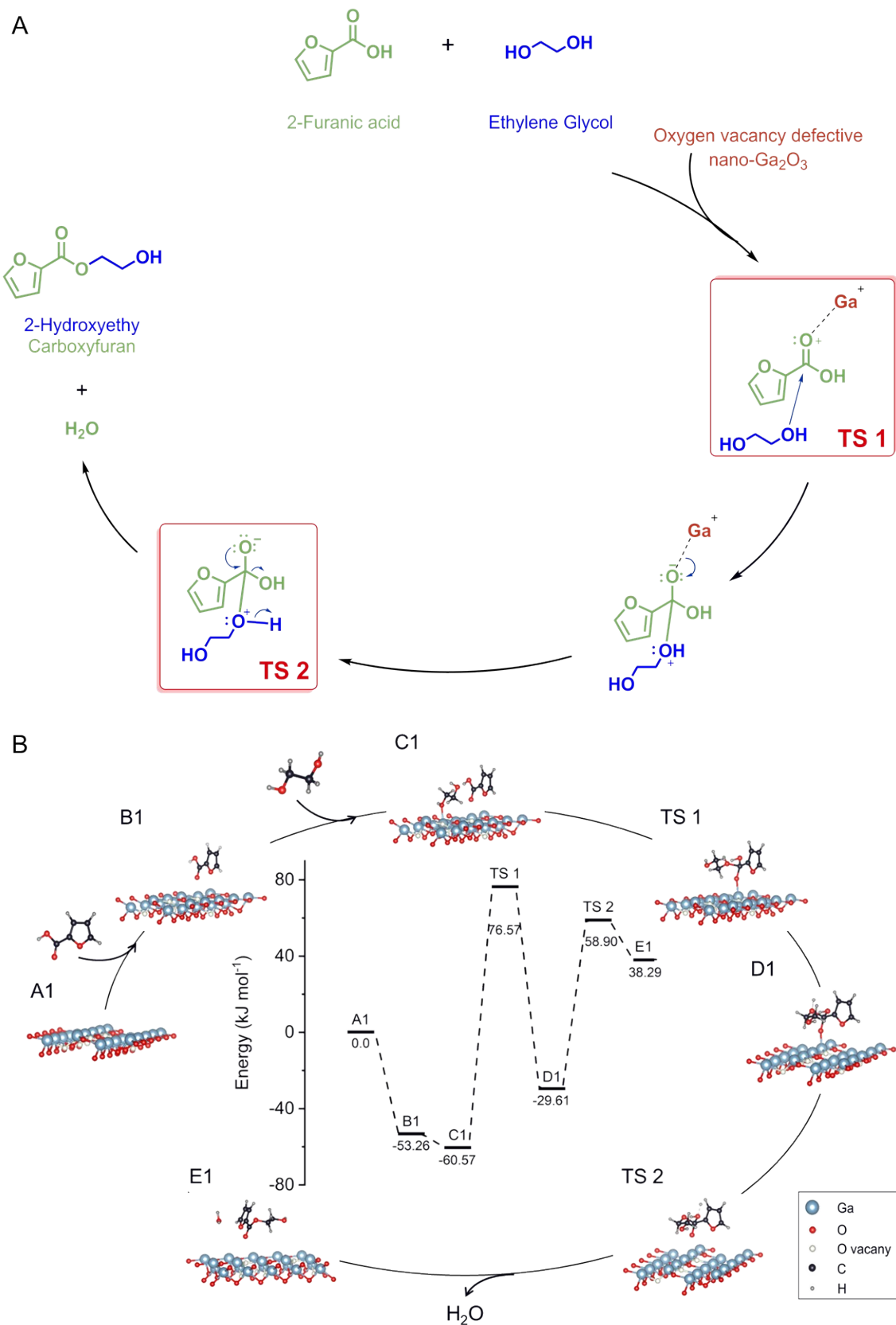
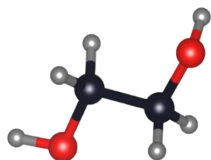
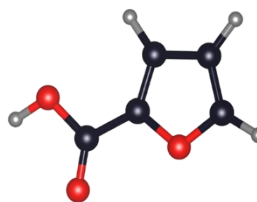


Fig. S16 (A) Modelled activation mechanism for the polymerization of PEF, using 2-Furanic acid to mimic PEF, ethylene glycol as a nucleophile, and oxygen-vacancy defective nano-Ga₂O₃ as catalyst, yielding 2-hydroxyethyl carboxyfuran and water as products; (B) Energy curve and reaction structure formula of 2-Furanic acid polymerization reaction pathway on oxygen-vacancy defective nano-Ga₂O₃ surface.

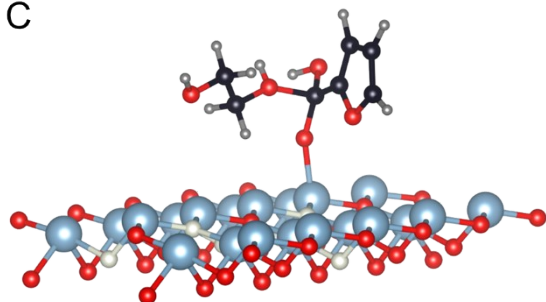
A



B



C



D

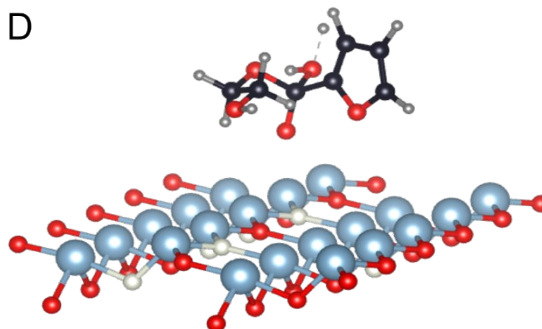


Fig. S17 Small molecular structure formula of (A) ethylene glycol and (B) 2-Furancarboxylic acid; the determined transition state structures for DFT computational optimization (C) TS 1 and (D) TS 2 (the blue, red, black, gray and white balls represent the Ga, O, C, H atoms, and oxygen vacancy).

Table. S1 Surface chemical composition of monolithic catalysts determined by XPS.

Catalysts	$V_{\text{O}}/O_{\text{Lattice}}$ ratio	$O_{\text{OH}^-}/V_{\text{O}}$
$\gamma\text{-Ga}_2\text{O}_3\text{-3}$	0.36	0.75
$\gamma\text{-Ga}_2\text{O}_3\text{-6}$	0.59	0.38
$\gamma\text{-Ga}_2\text{O}_3\text{-12}$	0.41	0.60

Table. S2 Atomic proportions of oxygen-vacancy defective nano $\gamma\text{-Ga}_2\text{O}_3\text{-n}$ catalysts (n represents the reflux reaction time in hours).

Catalysts	The atomic ratio of Ga to O
$\gamma\text{-Ga}_2\text{O}_3\text{-3}$	1:1.37
$\gamma\text{-Ga}_2\text{O}_3\text{-6}$	1:1.15
$\gamma\text{-Ga}_2\text{O}_3\text{-12}$	1:1.46

Table. S3 $\text{NH}_3\text{-TPD}$ data of oxygen-vacancy defective nano $\gamma\text{-Ga}_2\text{O}_3\text{-n}$ catalysts and $\beta\text{-Ga}_2\text{O}_3$ (n represents the reflux reaction time in hours).

Catalysts	Amount of adsorbed NH_3 ($\mu\text{mol g}^{-1}$)
$\gamma\text{-Ga}_2\text{O}_3\text{-3}$	172.55
$\gamma\text{-Ga}_2\text{O}_3\text{-6}$	376.02
$\gamma\text{-Ga}_2\text{O}_3\text{-12}$	254.74
$\beta\text{-Ga}_2\text{O}_3$	19.90

Table S4 Composition of PEF glycolysis products solid II.

PEF glycolysis products	Composition	Content (%)
Solid II	ethylene glycol	1.7
	diethylene glycol	0.6
	bis(hydroxyethyl)-2,5-furandicarboxylate (BHEFDC)	91.3
	BHEFDC dimer.	6.4

Table S5 The concentration of Ga_2O_3 in PEF after polymerization and repolymerization.

Samples	the concentration of Ga (ppm) ^a	the concentration of Ga_2O_3 (ppm) ^b
PEF	616	829
rPEF	762	1025

^a Measured by ICP-OES.

^b Calculated according to ICP-OES results.

Table. S6 Comparison of performances of rPEF and PEF.

Samples	M_n (kg mol ⁻¹)	M_w (kg mol ⁻¹)	\bar{D}	T_g (°C)	$T_{d-5\%}$ (°C)	T_{d-max} (°C)
PEF	41	74	1.83	86.0	374.1	424.4
rPEF	43	78	1.78	86.6	373.1	422.6

Table. S7 DFT calculations of adsorption energies between Ga₂O₃ and different groups of oxygen

Adsorption type	Adsorption energy (eV)
H ₂ O–Ga	0.302
furanyl O–Ga	-0.148
EG–Ga	-0.305
C=O–Ga	-0.583

The number of oxygen vacancies on Ga₂O₃ according to the reaction time

We synthesized γ -Ga₂O₃ samples with reflux reaction times of 1.5 h, 3 h, 6 h, 12 h, and 24 h, and used XPS analysis to compare the variations in oxygen vacancy content among these five samples. The results are shown in Fig S18 and Table S8. Specifically, as the reflux reaction time increases, the number of oxygen vacancies in γ -Ga₂O₃ shows a trend of increasing and then decreasing, and reaches the maximum at 6 h. The possible reasons for the specific trends in Ga₂O₃ nanoparticle size and oxygen vacancy defects observed at different reflux times are analyzed as follows:

Early Stage (1.5 h-6 h):

- **Particle Size:** During shorter reaction times, the rapid formation of nanocrystal nuclei occurs due to the high supersaturation in the system, resulting in the formation of a large number of small nuclei. As the reaction time extends (3-6 h), the particle size continues to decrease, which may be due to the dissolution of smaller particles and their subsequent deposition on the surfaces of other particles.
- **Oxygen Vacancy Defects:** At this stage, incomplete hydrolysis of reactants, along with rapid nucleation, may lead to an increase in oxygen vacancy defects. Between 3-6 h, the oxygen vacancy defects gradually increase, indicating that the defect structure on the nanoparticle surface and within

the crystal lattice is not yet stabilized. The 6 h mark is a critical point, at which the particle size reaches its minimum and the oxygen vacancy content is at its maximum, indicating the influence of surface irregularities and reaction conditions at this time.

Late Stage (6 h-24 h):

- **Particle Size:** After 6 h of reaction, the particle size begins to increase, which may be related to the advantage of larger particles in the Ostwald ripening process. Smaller particles gradually dissolve and transfer to larger particles through surface diffusion or precipitation.
- **Oxygen Vacancy Defects:** The concentration of oxygen vacancy defects begins to decrease as the crystal structure becomes more ordered, and the overall stability of the Ga₂O₃ improves.

Summary and Mechanistic Explanation:

- **Relationship Between Particle Size and Reaction Time:** The initial formation of small particles is linked to reactant concentration and supersaturation levels. As the reaction time increases, smaller particles are gradually replaced by larger ones due to dissolution and redeposition, leading to an initial decrease followed by an increase in particle size.
- **Dynamic Changes in Oxygen Vacancy Defects:** The increase in oxygen vacancies is closely related to surface energy and reaction time. During shorter reaction periods, incomplete reaction between GaCl₃ and water results in a high concentration of defects. However, longer reaction times promote crystal growth and structural stabilization, reducing the number of defects.
- **The 6 h Critical Point:** At 6 h, the particle size is at its minimum and the oxygen vacancy concentration is at its maximum, indicating a dynamic equilibrium in the system. Excessive reflux time leads to the formation and aggregation of more nanoparticle, improving the crystallinity of the particles.

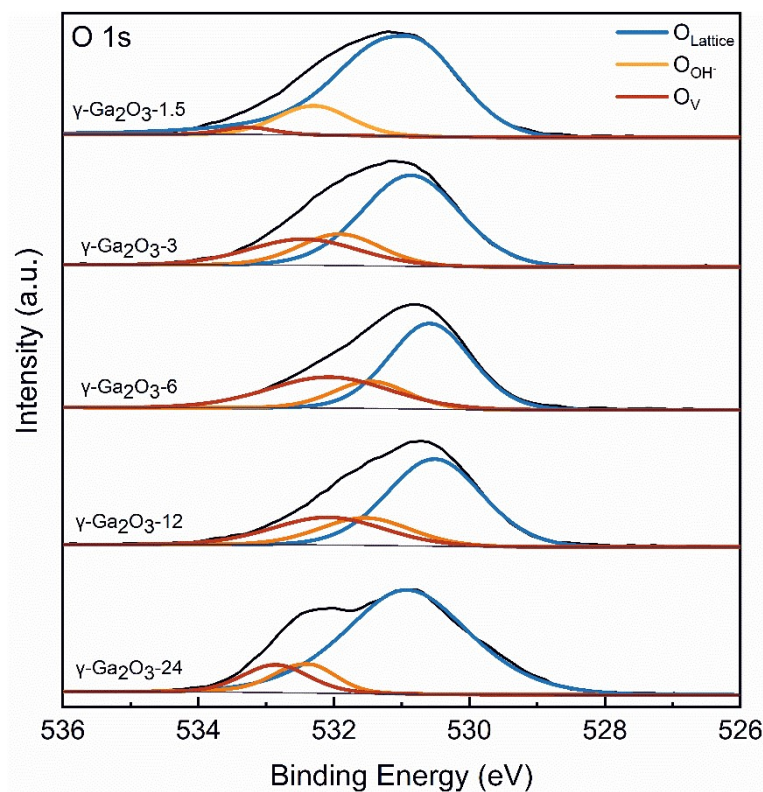


Fig. S18 O 1s spectra of $\gamma\text{-Ga}_2\text{O}_3\text{-}n$ (n represents the reflux reaction time in hours).

Table. S8 The content of different oxygen species in $\gamma\text{-Ga}_2\text{O}_3\text{-}n$ (n represents the reflux reaction time in hours).

Reflux reaction times (h)	$\text{O}_{\text{Lattice}}$ content (%)	O_{OH^-} content (%)	O_{V} content (%)
1.5	83.58	14.02	2.40
3	62.21	17.84	19.95
6	54.97	15.73	29.30
12	59.91	17.95	22.14
24	78.29	11.07	10.64

Turn-Over-Frequency (TOF) Calculations

(a) General concept

1. TOF of the catalyst = (mole of 2,5-furandicarboxylic acid conversion) / (mole of surface atoms of catalyst \times reaction time)
2. Since $\gamma\text{-Ga}_2\text{O}_3$ has a face-centred cubic structure with a lattice constant of 0.824 nm, the volume of unit cell in $\gamma\text{-Ga}_2\text{O}_3$ nanocrystals is $(0.824 \text{ nm})^3 = 0.559 \text{ nm}^3$. Each unit cell contains 4 Ga atoms.
3. A cube with an edge length of b has a surface area of $6 b^2$ and a volume of b^3 .
4. $\gamma\text{-Ga}_2\text{O}_3$ nanocube is enclosed by $\{100\}$ facet. Each two-dimensional unit cell on the $\{100\}$ facets contains 2 Ga atoms. The area of this unit cell is $(0.824 \text{ nm})^2 = 0.679 \text{ nm}^2$.

(b) Number of Ga atoms in each γ -Ga₂O₃ nanocrystals

Number of Ga atoms in each cubic γ -Ga₂O₃ nanocrystals = (volume of each nanocube / volume of each unit

$$\text{cell}) \times \text{atoms in each unit cell} = \left(\frac{b^3}{0.559} \right) \times 4 = 7.156 \times b^3$$

(c) Number of Ga atoms on the surface of each γ -Ga₂O₃ nanocrystals

Number of Ga atoms on the surface of each cubic γ -Ga₂O₃ nanocrystals = (surface area of each nanocube / surface area of each two-dimensional unit cell on the {100} facets) \times atoms in each two-dimensional unit cell

$$\text{on the } \{100\} \text{ facets} = \left(\frac{6 \times b^2}{0.679} \right) \times 2 = 17.673 \times b^2$$

(d) Mole of surface atoms of γ -Ga₂O₃ catalyst

Mole of surface atoms of cubic γ -Ga₂O₃ nanocrystals = (Number of Ga atoms on the surface of each cubic γ -Ga₂O₃ nanocrystals / number of Ga atoms in each cubic γ -Ga₂O₃ nanocrystals) \times mole of cubic γ -Ga₂O₃

$$\text{nanocrystals} = \left(\frac{17.673 \times b^2}{7.156 \times b^3} \right) \times 5 \times 10^{-5} = 1.235 \times 10^{-4} \times \frac{1}{b}$$

(e) Summary for the calculations

Catalysts	Morphology	Average size	Mole of surface atoms	t_c^a	TOF
γ -Ga ₂ O ₃ -3	Cube	9.2 nm	1.34×10^{-5} mol	3.1 h	1204 h ⁻¹
γ -Ga ₂ O ₃ -6	Cube	7.9 nm	1.56×10^{-5} mol	2.1 h	1526 h ⁻¹
γ -Ga ₂ O ₃ -12	Cube	10.9 nm	1.13×10^{-5} mol	3.0 h	1475 h ⁻¹
β -Ga ₂ O ₃	Monoclinic	40.0 nm	4.13×10^{-6} mol	4.1 h	2953 h ⁻¹
TBT	-	-	-	2.7 h	370 h ⁻¹

^a Time needed to reach the clear point in the esterification stage.